

Constrained Workspace Generation for Snake-like Manipulators with Applications to Minimally Invasive Surgery

Ryan J. Murphy^{1,2}, Matthew S. Moses¹, Michael D. M. Kutzer¹, Gregory S. Chirikjian², and Mehran Armand^{1,2}

Abstract—Osteolysis is a debilitating condition that can occur behind the acetabular component of total hip replacements due to wear of the polyethylene liner. Conventional treatment techniques suggest replacing the component, while less-invasive approaches attempt to access and clean the lesion through the screw holes in the component. However, current rigid tools have been shown to access at most 50% of the lesion. Using a recently developed dexterous manipulator, we have adapted a group-theoretic convolution framework to define the manipulator’s workspace and its ability to fully explore a lesion. We compared this with the experimental exploration of a printed model of the lesion. This convolution approach successfully contains the experimental results and shows over 98.8% volumetric coverage of a complex lesion. The results suggest this manipulator as a possible solution to accessing much of the area unreachable to the conventional less-invasive technique.

I. INTRODUCTION

Previously, we have developed and characterized an underactuated, snake-like manipulator [1]. Two nested tubes of superelastic nitinol form the structure of the manipulator while a pull-pull cable mechanism provides the actuation. This continuum robot bends in a single plane, with the ability to resist high out-of-plane forces, and can reach bends exceeding 180° [2].

One potential application for the manipulator is to remove osteolysis from behind the acetabular component of total hip arthroplasties (THA) during a revision surgery. Osteolysis is bone degradation that has been associated with the release of wear particles from the polyethylene liner in the THA. The invasive treatment for osteolysis behind the acetabular component of a THA involves replacing said component, cleaning the lesion, and grafting the bone behind the implant. During the THA revision surgery, if the acetabular component is not loose, osteolysis can be treated with a less-invasive approach that preserves the existing well-fixed acetabular component. In this approach, surgeons access the region behind the implant via the screw holes in the acetabular component.

*This work was supported in part by Independent Research and Development funds provided by the Johns Hopkins University Applied Physics Laboratory.

¹R. J. Murphy, M. S. Moses, M. D. M. Kutzer, and M. Armand are with the Research and Exploratory Development Department, Johns Hopkins University Applied Physics Laboratory, Laurel, MD, USA {Ryan.Murphy, Matthew.Moses, Michael.Kutzer, Mehran.Armand}@jhuapl.edu

²R. J. Murphy, G. S. Chirikjian, and M. Armand are with the Department of Mechanical Engineering, Johns Hopkins University, Baltimore, MD, USA {rjmurphy, marmand2, gchirikj1}@jhu.edu

Engh et. al [3] suggest that surgeons can typically remove no more than 50% of the lesion through the conventional less-invasive approach. Our manipulator was designed with an outer diameter of 5.99 mm to enter through the screw holes of the acetabular component and explore the lesion in a similar fashion to the conventional less-invasive approach. Using the 4 mm lumen, we can pass tools (e.g. brushes, water jets, vacuums) through the manipulator to explore and interact with the cavity. The previous application of a path planning simulation relying on the ability that the manipulator detect collisions with the lesion wall proved the effectiveness of our manipulator in dynamically exploring various lesion geometries [4]. While successfully showing significant exploration of difficult cavities (over 85%), this path-planning approach neither defines nor considers the entire workspace of the manipulator, employs a simplified kinematic model of the manipulator, and is used assuming no prior cavity model. Moreover, the previous path-planning approach relies on nonexistent sensors attached to the manipulator to detect collisions with the lesion wall,

Several variations on snake-like manipulators have previously been described (e.g. [5]–[7]). Previous work demonstrated an efficient, group-theoretic approach for defining a manipulator’s workspace [8]–[10]. This method uses a convolution technique to efficiently generate an approximate workspace for an articulated system. This approach was originally developed for discrete actuators, but can be applied to continuum robots such as the current manipulator by discretizing the actuation over the realm of possible states that can or cannot be reached by actuation alone. Moreover, these works do not consider obstacles in the workspace.

A thorough understanding of the region reachable by the manipulator contained inside a particular lesion geometry yields many possibilities for improved surgical outcomes. First, one can preoperatively estimate the effectiveness of using the manipulator to clean the lesion. If deemed ineffective, a surgeon may decide to perform a full total hip revision as opposed to cleaning the lesion. One can also determine the necessity (and utility) of adding a second insertion portal (e.g., through the pelvis) to clean the lesion.

In this paper, we present a brief review of the manipulator and group convolution. We leverage group-theoretic convolution to define the workspace of this manipulator and use these techniques to estimate the total lesion coverage we can achieve. Using simple experimental data, we validate the computed workspace and lesion coverage. The presented

technique can be used to quickly evaluate the performance of a manipulator given a model of the lesion.

II. BACKGROUND

This section briefly reviews some pertinent background material. First, the manipulator kinematics are described. Next, we provide a brief overview of convolution on groups.

A. Kinematics

Compared to the prior kinematic model of the manipulator (a dual backbone approach [1]), we have modeled the manipulator here as a single chain of 27 pin joints (Fig. 1). The kinematic approach presented below compares well with dual backbone approach and tracks well with experimental data. The use of the single chain in this study simplifies the group-theoretic convolution used to define the manipulator workspace.

Other snake-like manipulators (e.g. [11]–[15]) employ a backbone curve approach developed by Chirikjian and Burdick [16] to model the kinematics of their respective manipulators. In part, this is due to the construction and geometry of these manipulators. Without structural integrity and notable “joints,” the conventional rigid link approach breaks down. However, our manipulator’s structural integrity, geometry, and apparent joint structure lends itself to this single chain kinematic model.

Planar rigid-body rotation about a pin joint, $g \in SE(2)$ can be modeled as

$$g(x, y, \theta) = \begin{bmatrix} \cos \theta & -\sin \theta & x \\ \sin \theta & \cos \theta & y \\ 0 & 0 & 1 \end{bmatrix}, \quad (1)$$

In our single chain model, the rotation about the i^{th} pin joint, γ_i , is defined as $h_i(\gamma_i) = g(-l_i \sin \gamma_i, l_i \cos \gamma_i, \gamma_i)$. Here, l_i is geometrically defined as 1.21 mm for $i \in \{1, 2, \dots, 26\}$ and $l_{27} = 2.62$ mm. In this case, h_{27} is the transformation from the 27^{th} pin joint to the center of the tip of the manipulator.

B. Convolution

Convolution of probability density functions (PDF) $\rho_1(g)$ and $\rho_2(g)$ mapping $SE(2)$ to \mathbb{R} on $SE(2)$ is defined as

$$(\rho_1 * \rho_2)(g(x, y, \theta)) = \int_{SE(2)} \rho_1(g(\xi, \eta, \alpha)) \rho_2(g(\xi, \eta, \alpha))^{-1} g(x, y, \theta) d\mu(g(\xi, \eta, \alpha)) \quad (2)$$

where $d\mu(g(\xi, \eta, \alpha))$ is a differential volume element of $SE(2)$. In our case, we discretize over $SE(2)$ (and, as such, any associated $\rho(g)$) and approximate the convolution integral of histograms $f_1(g)$ and $f_2(g)$, which are the discretized versions of $\rho_1(g)$ and $\rho_2(g)$, as a Riemann-Stieltjes sum [8].

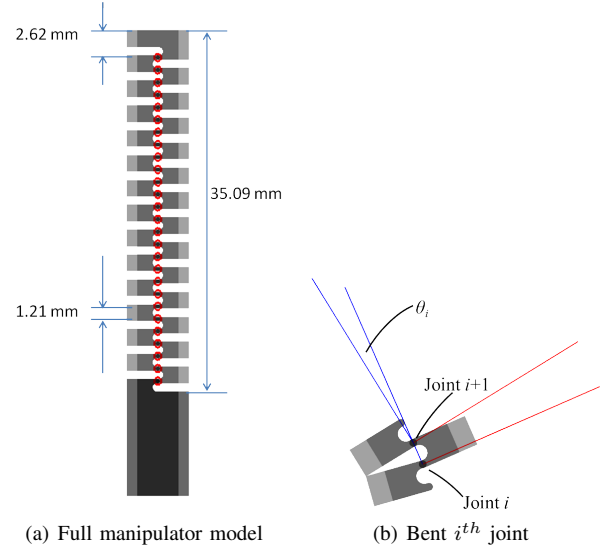


Fig. 1. Geometric and kinematic model of the manipulator. The pin joints are located at the center of the red circles.

We define $f_i(x, y, \theta) = f_i(g(x, y, \theta))$ for $i \in \{1, 2\}$. Here,

$$\begin{aligned} & (\rho_1 * \rho_2)(g(x, y, \theta)) \\ & \approx \sum_{l=0}^{N_1} \sum_{m=0}^{N_2} \sum_{n=0}^M f_1(\xi_l, \eta_m, \alpha_n) \cdot f_2((x - \xi_l) \cos \alpha_n \\ & + (y - \eta_m) \sin \alpha_n, -(x - \xi_l) \sin \alpha_n + (y - \eta_m) \\ & \cos \alpha_n, (\theta - \alpha_n) \bmod 2\pi) \Delta \xi \Delta \eta \Delta \alpha, \end{aligned} \quad (3)$$

with N_1 , N_2 , and M representing the number of discretizations in x , y , and θ , respectively. Given bounds on the parameters, we define $\Delta \xi = (x_{max} - x_{min})/N_1$, $\Delta \eta = (y_{max} - y_{min})/N_2$, and $\Delta \alpha = (\theta_{max} - \theta_{min})/M$.

III. METHODS

The underactuated manipulator is controlled via two stainless steel cables traveling through channels on either side of the manipulator. Pulling these cables actuates the manipulator, causing C-shaped bends in a single bend plane (Fig. 2). This section describes the characterization of both a *restrictive* (disallowing self-collisions) and *non-restrictive* workspace, the experimental exploration of a specific lesion geometry, and the simulated exploration of that same geometry.

A. Unobstructed Workspace Generation

We performed two different convolutions to generate two workspaces using the presented technique: a *restrictive* and a *nonrestrictive* workspace. The *restrictive* workspace ensures no self-collisions occur along the manipulator (i.e. the manipulator does not bend back on itself). The *nonrestrictive* workspace does not check for self-collisions, allowing the maximum bend at each joint. Due to the geometry of the manipulator, the maximum theoretical bend a single pin joint can achieve is approximately 15.8° . At this magnitude of bend, a collision will occur and any further bend will not be possible. This is the only constraint on the *nonrestrictive*

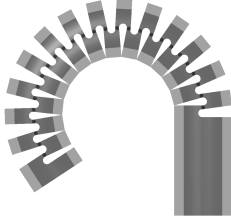


Fig. 2. Bent configuration (each joint at 7.9 degrees), indicating no collisions.

workspace. However, if the bend joint i is 7.9° and the bend of joint $i + 1$ is at least 7.9° (or vice versa), a self-collision will also result. To achieve this restriction, we appropriately bounded γ such that, for any set of two links, collisions would not occur. Specifically, $\gamma_{min} = -7.9^\circ$ and $\gamma_{max} = 7.9^\circ$ (except for the first link, which was bounded by $\gamma \in [-15.8, 7.9]$). The choice of θ for the *restrictive* workspace guarantees no self-collisions of the manipulator, even in the presence of external forces. It is possible to choose different γ_i limits than those presented; however, our choice represents the largest possible workspace without collision (Fig. 2). In the *non-restrictive* workspace, we allowed the full absolute bend of 15.8° for each link.

For both the restrictive and non-restrictive workspace generations, we followed the same approach to perform the convolution. Since there are 25 identical modules, we performed the following sets of convolutions:

$$\begin{aligned}
f_2 &= f_l^2 * f_l^2 \\
f_4 &= f_2 * f_2 \\
f_8 &= f_4 * f_4 \\
f_{16} &= f_8 * f_8 \\
f_{24} &= f_{16} * f_8 \\
f_{25} &= f_{24} * f_l^2 \\
f_{26} &= f_{25} * f_l^1 \\
f_{27} &= f_{26} * f_l^{27}
\end{aligned} \tag{4}$$

Each f is a discretized density map such that $f(g) \neq 0$ if the link can reach the location specified by $g \in SE(2)$. The specific bounds and discretization for f are a function of the number of links being convolved, n , and the γ bounds on the i^{th} link, γ_i . The histogram of each link segment is defined by f_l^i ; the beginning link is f_l^1 , the end link is f_l^{27} , and all other links ($i \in \{2, 3, \dots, 26\}$) are identical.

$$x_{min} = \sum_{i=1}^n l_i * \sin \left(\max \left(\sum_{j=1}^i \gamma_j^{min}, -\pi/2 \right) \right) \tag{5}$$

$$x_{max} = \sum_{i=1}^n l_i * \sin \left(\min \left(\sum_{j=1}^i \gamma_j^{max}, \pi/2 \right) \right) \tag{6}$$

$$y_{min} = \sum_{i=1}^n l_i * \cos \left(\max \left(\sum_{j=1}^i \gamma_j^{min}, -\pi \right) \right) \tag{7}$$

$$y_{max} = \sum_{i=1}^n l_i \tag{8}$$

$$\theta_{min} = \max \left(\sum_{j=1}^i \gamma_j^{min}, -\pi \right) \tag{9}$$

$$\theta_{max} = \min \left(\sum_{j=1}^i \gamma_j^{max}, \pi \right) \tag{10}$$

The manipulator maintains *C-shaped* bends in the absence of external forces due to the pull-pull actuation mechanism. These *C-shaped* bends represent the outermost boundary of the workspace of the manipulator. Specifically, they define the outer bounding curve for all other complex *S-shaped* bends that occur due to external forces. We used this outer boundary of *C-shaped* bends to compare against the outer boundary of the workspaces generated via convolution.

To construct the experimental bound, we freely bent the manipulator while maintaining zero tension in the non-driving cable. To reduce the potential for cable breakage, we enforced a maximum force of 33.4 N on either cable. Starting at a zero-tension position, we pulled the left cable until reaching the maximum force, released the left cable until returning to zero-tension, and then actuated the right cable to maximum force.

The movement was recorded by an overhead camera (Fig. 3) and we used an image processing method to define the manipulator skeleton. From the skeleton, we estimated the manipulator kinematics and defined the tip position in the manipulator coordinate space.

B. Experimental Lesion Exploration

One goal of the manipulator is to explore osteolytic lesions forming behind the acetabular component of total hip replacements. The lesions are due, in part, to wear particles formed from the polyethylene liner and cause the bone to degrade. We developed a simple “ant farm” approach for testing lesion exploration using a surgically-relevant lesion [4]. First, from a defined lesion geometry behind an acetabular component, we identified two access points and axes corresponding to the two screw holes in the acetabular component. Since the motion of the manipulator is constrained to a single “bend plane,” we constructed a series of slice planes about each of the available insertion axes (Fig. 4). Each slice plane was offset from the insertion axis by 4.00 mm creating a total slice thickness of 8.00 mm, which is slightly larger than

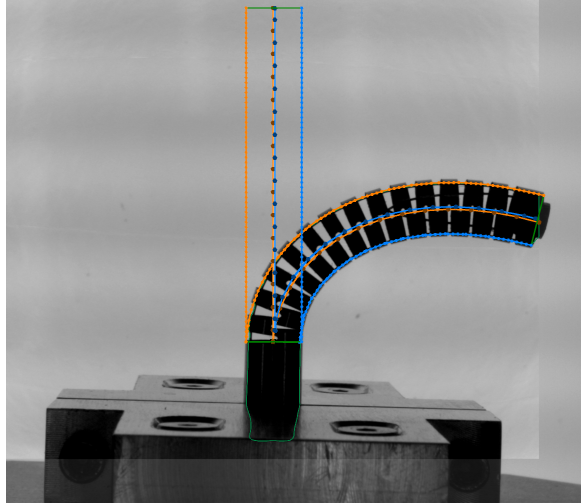


Fig. 3. Sample image from a free manipulator bend with the extracted skeleton overlaid.



Fig. 4. Sample planar slice showing manipulator entering through screw hole.

the diameter of the manipulator. This “ant farm” approach allowed us to deconstruct a complex 3D geometry into a series of simple, planar slices the manipulator could easily interact with using only the in-plane bending capabilities.

Using a Spectrum Z™ 510 (Z Corporation, Burlington, MA), we printed each of the slices. Two sheets of acrylic clamped the slices to the test setup and a user manually explored the lesion. The goal of this exploration was to follow the perimeter wall as closely as possible for each slice. We recorded the exploration of each slice using an overhead camera. In each image, we manually identified the tip position and orientation of the manipulator from three digitized points and manually registered the 3D slice to the image. We performed this exploration procedure over ten slices through each of the two available access points in the acetabular implant (20 slice planes in total) 5.

To evaluate the perimeter coverage of the manipulator, we found the closest face of the lesion geometry to each of the manipulator tip points defined through the lesion exploration.

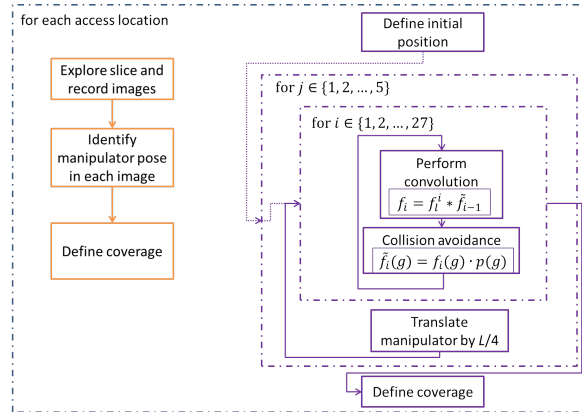


Fig. 5. Algorithmic flowchart for a single slice for the experimental (orange) and simulation (purple) approached.

If this face was within 3.00 mm of the manipulator tip position, we identified that face as having been touched. This distance was chosen since it reflects the manipulator radius. We compared the surface area of the touched faces with the total surface area of the lesion. The assumption is faces further away are not touched since the manipulator must come to a hard stop once it begins to interact with the lesion surface.

C. Simulated Lesion Exploration

Since the manipulator can be translated in and out of the lesion, we discretized the manipulator into five translational states: incrementing from the initial insertion to the full manipulator insertion by one-quarter lengths of the manipulator. At each translation step, we performed a link-by-link convolution of the manipulator. After each convolution, we bounded the result using the lesion shape (Fig. 5). Specifically, for each potential convolution location, we ensured this location was either (1) due to an unbent configuration or (2) was contained within the lesion space.

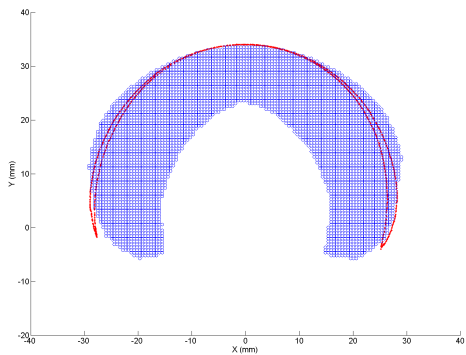
For our approach, we transformed the lesion geometry such that the y-axis aligned with the translational axis of the manipulator and defined the origin appropriately for each specific manipulator translation. The first condition (an unbent configuration) constrains the manipulator to an unbent state when it is outside the lesion. This is specifically useful before the manipulator has fully entered the lesion. The second condition truncates each convolution to remain within the lesion geometry.

$$f_i = f_l^i * \tilde{f}_{i-1} \quad (11)$$

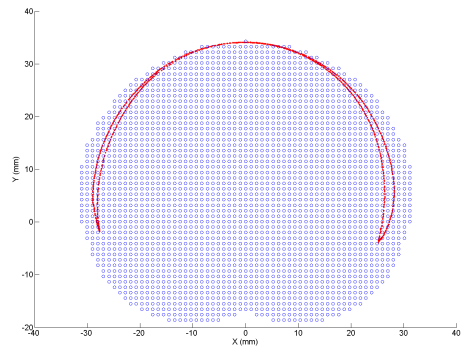
$$\tilde{f}_i(g) = f_i(g) \cdot p(g) \quad (12)$$

$$p(g(x, y, \theta)) = \begin{cases} 1 & (x, y)^T \in P \\ 0 & (x, y)^T \notin P \end{cases} \quad (13)$$

Here, \tilde{f} is the truncated convolution, f_l^i is the histogram of the i^{th} link, and $p(g(x, y, \theta))$ is the logical representation of the polygon P where the θ aspect of g is ignored. The final states $\tilde{f}_i(g)$ indicated the reachable configuration of the manipulator.



(a) Restrictive workspace guaranteeing no self-collisions



(b) Non-restrictive workspace allowing self-collisions

Fig. 6. Planar manipulator unobstructed workspace (blue) with experimentally generated workspace bounds overlaid in red.

To identify the volumetric coverage, we voxelized the lesion geometry into 0.1 mm cubic voxels. For each manipulator point, we identified the corresponding voxel the manipulator entered. However, this procedure only accounts for the tip of the manipulator. To account for the manipulator size, we add a 3.00 mm radius ball around each point of the manipulator tip and assess the coverage from this set of points. To add the ball, we voxelized the ball into 0.1 mm cubic voxels to match the size of the lesion voxels. We performed a convolution of the manipulator volume with the ball volume to define the workspace of the manipulator. By comparing the voxelized lesion geometry with that of the manipulator, we define the total volumetric coverage of the manipulator.

Using the voxelized representation of our workspace, we evaluated the perimeter coverage of the simulation in the same way as we did for the experiment. That is, we identified the closest face (within 2.90 mm accounting for the voxel size) of the voxel. Accumulating the faces over the simulation provided an estimate of the perimeter coverage that is comparable to the experimental results.

IV. RESULTS

A. Unobstructed Workspace

The outer envelope of both the restrictive and non-restrictive workspaces matched very well with the exper-

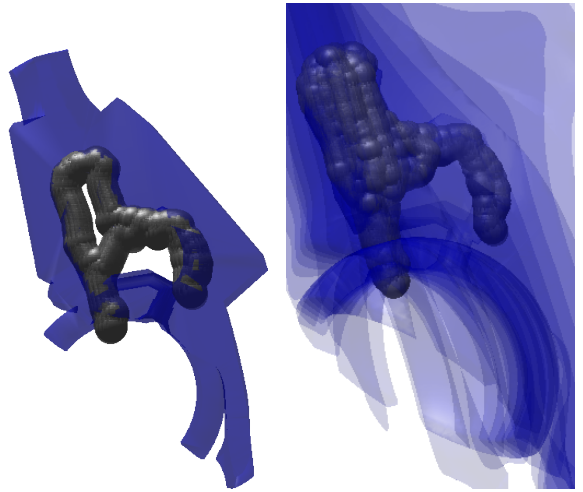


Fig. 7. Experimental results showing the lesion and cup model (blue) and the end effector of the manipulator through time (gray).

imental results (Fig. 6). As expected, the non-restrictive workspace folded back on itself and, as such, suffered self-collisions. The restrictive workspace avoided this folding back and sees maximum bends almost equivalent to that of the experimental data.

B. Lesion Exploration

1) *Experimental:* The experimental manipulator exploration covered 2581 mm² of the 2738 mm² (94.4%) of the cavity surface area. Of the 4740 faces in our model, 216 were untouched (Fig. 7). The first access point left 1614 faces untouched, while the second left 2104 untouched. The two access points overlapped to touch 1238 of the same faces in the model.

2) *Simulated:* The simulated manipulator exploration covered 2724 mm² of the 2738 mm² (99.5%) of the cavity surface area. Of the 4740 faces in our model, 21 were untouched. The simulation achieved 7.45×10^7 mm³ of the 7.54×10^7 mm³ (98.8%) coverage of the lesion volume (Fig. 8). A comparison with the experimental results show the simulation successfully encapsulated the experimental data for lesion exploration (Fig. 9).

V. DISCUSSION AND CONCLUSION

We presented a modified group-theoretic convolution approach to compute a manipulator workspace in a region with obstacles and convex boundaries, specifically that of an osteolytic lesion behind a total hip replacement. The comparison between experimental and simulated results defining the workspace for a snake-like manipulator validated the approach. We have shown the effective exploration of a specific lesion geometry, demonstrating utility of the manipulator in a surgical scenario. The presented method can be useful for optimizing over design parameters when designing new manipulators for other tasks, ensuring the reachability and effectiveness in particular environments containing obstacles or bounds.

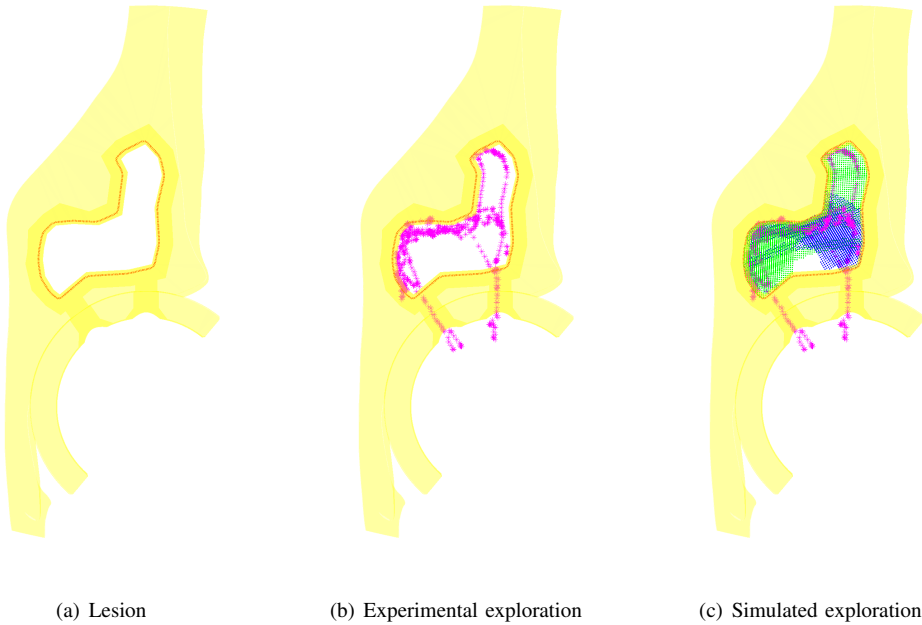


Fig. 9. Sample simulated (blue/green for different access points) and experimental (magenta) lesion exploration with the boundaries in red.

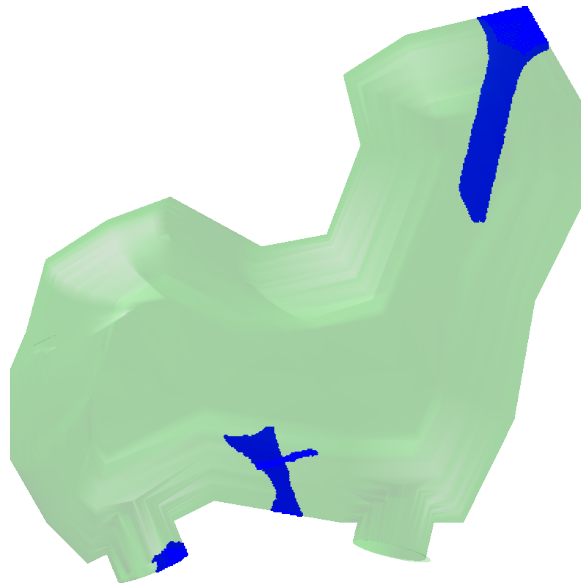


Fig. 8. Simulated coverage of the lesion. The blue points indicate inaccessible regions.

Predictably, the experimentally-defined workspace was near the outer envelope of the convolution-defined workspace. This matches intuition since no external forces were applied during the experiment, thereby allowing full C-shaped bends. However, the restrictive workspace does not entirely capture the experimental data recorded from the tip of the manipulator (Fig. 6). This is not surprising as, by definition of the restrictive workspace, we know that certain valid manipulator configurations are not included.

One potential way to refine the workspace estimate is to develop a technique for defining self-collisions. Nonetheless, the non-restrictive workspace fully encapsulates the experimental data.

The experimental exploration of the lesion slice was done with rudimentary control over the manipulator and no prior planning. Nonetheless, the experimental results of 94.4% coverage along the lesion boundary lend credence to the applicability of this manipulator for exploring a surgically-relevant bone lesion [4]. A user bent and translated the manipulator through the lesion with the goal to cover as much perimeter as possible without regard to the interior area of the lesion. As such, the simulated coverage was greater than the experimental coverage (Fig. 9). Moreover, parts of the lesion were inaccessible to the manipulator due to an increased wall thickness (the manipulator could not translate to the space) and this was not taken into consideration when performing the convolution simulation. Nonetheless, the simulation reveals that we can effectively explore a lesion and achieve coverage much greater than that of the conventional technique.

Comparatively, the simulation overestimated the coverage defined by the experimental data. There are a variety of reasons why this is the case. Both the simulation and the experiment contain sources of error. The experiment was manually controlled and manually analyzed. The simulation treated the manipulator as a simple line segment instead of using the true cylindrical shape, which will impact the reachability at the outer boundaries of the convolution, reducing the total workspace.

Although the simulated coverage estimate was performed

at discrete translations into the lesion, the high coverage (98.8%) of the volume indicates the manipulator is very effective in exploring the lesion. The simulation included the same perimeter region as the experimental results, further validating the bounded convolution approach taken in this work. Given that surgeons can typically only ensure about 50% coverage, this is a remarkable improvement.

This study assumes that all the joints of the manipulator are independent. However, this is not the case for a free bend without countertension or external forces. Preliminary work in developing a dynamic model of the manipulator suggests that without any external forces, the absolute bend angle at joint i must be less than or equal to that of joint $i-1$ and the signs of these angles must be the same. We performed all convolutions assuming external forces could be applied at any location on the manipulator. In reality, this may not be the case and leads to overestimation of lesion coverage. Additionally, we maintained maximum joint angle bends of $\pm 7.9^\circ$ to ensure that no self-collisions occurred.

Future work includes modifying the convolution technique to directly assess the 3D coverage of the manipulator instead of following this 2D slice approach. Doing so will include more accurate results. We intend to explore including the 5.99 mm diameter of the manipulator in the convolution. The present work treated the manipulator as a segmented line through space. That is, we ignored the diameter of the manipulator when assessing collisions with the lesion boundary. Improving the convolution to account for the manipulator dimensions has the potential to coverage around the edges and at extreme bends. One possible way to estimate this coverage is to “bubble” in the lesion, allowing the treatment of the manipulator as a segmented line. A similar convolution approach was taken by Mason and Burdick [17] and used to perform motion planning. We could adapt this approach to plan the exploration of a lesion.

In conclusion, we have presented a group-theoretic approach to define the workspace for an underactuated, snake-like manipulator. We demonstrated that such an approach encapsulates experimental data. We used a modified version of the convolution technique to define the total possible coverage in a sample osteolytic lesion behind a total hip arthroplasty. The results indicate the feasibility of this manipulator as a potential solution to accessing much of the area unreachable to the conventional technique. We believe this work can be a great asset in helping to plan and execute the exploration of a lesion to remove osteolysis.

VI. ACKNOWLEDGMENTS

The authors would like to gratefully acknowledge Dr. Kevin Wolfe for his review of this work, and Mr. Sean

Segreti and Mr. Chester Chambers for their contributions to experimentation.

REFERENCES

- [1] M. D. M. Kutzer, S. M. Segreti, C. Y. Brown, M. Armand, R. H. Taylor, and S. C. Mears, “Design of a new cable-driven manipulator with a large open lumen: Preliminary applications in the minimally-invasive removal of osteolysis,” in *Proc. IEEE Int Robotics and Automation (ICRA) Conf.*, 2011, pp. 2913–2920.
- [2] M. D. M. Kutzer, “Advances in cooperative robotics,” PhD, Johns Hopkins University, 2012.
- [3] C. A. Engh, Jr., H. Egawa, S. E. Beykirch, R. H. Hopper Jr., and C. A. Engh, “The quality of osteolysis grafting with cementless acetabular component retention,” *Clin Orthop Relat Res*, vol. 465, pp. 150–154, Dec. 2007.
- [4] W. P. Liu, B. C. Lucas, K. Guerin, and E. Plaku, “Sensor and sampling-based motion planning for minimally invasive robotic exploration of osteolytic lesions,” in *Proc. IEEE/RSJ Int Intelligent Robots and Systems (IROS) Conf.*, 2011, pp. 1346–1352.
- [5] S. Hirose, *Biologically Inspired Robots: Snake-like Locomotors and Manipulators*. Oxford, U.K.: Oxford University Press, 1993.
- [6] I. D. Walker and M. W. Hannan, “A novel ‘elephant’s trunk’ robot,” in *Proc. IEEE/ASME Int Advanced Intelligent Mechatronics Conf.*, 1999, pp. 410–415.
- [7] C. Wright, A. Johnson, A. Peck, Z. McCord, A. Naaktgeboren, P. Giangrande, M. Gonzalez-Rivero, R. Hatton, and H. Choset, “Design of a modular snake robot,” in *Proc. IEEE/RSJ Int. Conf. Intelligent Robots and Systems (IROS) Conf.*, 2007, pp. 2609–2614.
- [8] G. S. Chirikjian and I. Ebert-Uphoff, “Numerical convolution on the euclidean group with application to workspace generation,” *IEEE Transactions on Robotics and Automation*, vol. 14, no. 1, pp. 123–136, February 1998.
- [9] I. Ebert-Uphoff and G. S. Chirikjian, “Efficient workspace generation for binary manipulators with many actuators,” *Journal of Robotic Systems*, vol. 12, no. 6, pp. 383–400, 1995.
- [10] Y. Wang and G. S. Chirikjian, “Workspace generation of hyper-redundant manipulators as a diffusion process on se(n),” *IEEE Transactions on Robotics and Automation*, vol. 20, no. 3, pp. 399–408, 2004.
- [11] I. A. Gravagne and I. D. Walker, “On the kinematics of remotely-actuated continuum robots,” in *Proc. IEEE Int. Conf. Robotics and Automation ICRA ’00*, vol. 3, 2000, pp. 2544–2550.
- [12] P. Sears and P. Dupont, “Inverse kinematics of concentric tube steerable needles,” in *Proc. IEEE Int Robotics and Automation (ICRA) Conf.*, Apr. 2007, pp. 1887–1892.
- [13] N. Simaan, R. Taylor, and P. Flint, “A dexterous system for laryngeal surgery,” in *Proc. IEEE Int Robotics and Automation (ICRA) Conf.*, vol. 1, 2004, pp. 351–357.
- [14] N. Simaan, K. Xu, W. Wei, A. Kapoor, P. Kazanzides, R. Taylor, and P. Flint, “Design and integration of a telorobotic system for minimally invasive surgery of the throat,” *The International Journal of Robotics Research*, vol. 28, no. 9, pp. 1134–1153, Sep. 2009.
- [15] R. Webster, J. Romano, and N. Cowan, “Mechanics of precurved-tube continuum robots,” *IEEE Transactions on Robotics*, vol. 25, no. 1, pp. 67–78, Feb. 2009.
- [16] G. S. Chirikjian and J. W. Burdick, “Kinematically optimal hyper-redundant manipulator configurations,” *IEEE Transactions on Robotics and Automation*, vol. 11, no. 6, pp. 794–806, 1995.
- [17] R. Mason and J. W. Burdick, “Trajectory planning using reachable-state density functions,” in *Proc. IEEE Int Robotics and Automation (ICRA) Conf.*. Springer, 2002, pp. 273–280.